Robust Model-Based Fault Diagnosis for PEM Fuel Cell Air-Feed System

Jianxing Liu, Wensheng Luo, Xiaozhan Yang and Ligang Wu, *Senior Member, IEEE*

***Abstract*—In this paper, the design of a nonlinear observer-based fault diagnosis approach for polymer electrolyte membrane (PEM) fuel cell air feed systems is presented, taking into account a fault scenario of sudden air leak in the air supply manifold. Based on a simplified nonlinear model proposed in the literature, a modified super-twisting (ST) sliding mode algorithm is employed to the observer design. The proposed ST observer can estimate not only the system states, but also the fault signal. Then, the residual signal is computed on-line from comparisons between the oxygen excess ratio obtained from the system model and the observer system, respectively. Equivalent output error injection using the residual signal is able to reconstruct the fault signal, which is critical in both fuel cell control design and fault detection. Finally, the proposed observer-based fault diagnosis approach is implemented on the Matlab/Simulink environment in order to verify its effectiveness and robustness in the presence of load variation.**

***Index Terms*—PEM fuel cells; fault diagnosis; super-twisting algorithm.**

NOMENCLATURE

η_{cm}	Motor mechanical efficiency
η_{cp}	Compressor efficiency
γ	Ratio of specific heats of air
ω_{atm}	Relative humidity of the ambient air
$\omega_{\text{ca,in}}$	Relative humidity of the inlet air
A_T	Operating area of the nozzle
A_{fc}	Active area
C_D	Discharge of the nozzle
C_p	Constant pressure specific heat of air
F	Faraday constant
J_{cp}	Compressor inertia
k_t	Motor constant
$k_{\text{ca,in}}$	Cathode inlet orifice constant
M_v	Vapor molar mass
M_{N_2}	Nitrogen molar mass
M_{O_2}	Oxygen molar mass
n	Number of cells in fuel cell stack
p_{atm}	Atmospheric pressure
R	Universal gas constant
T_{atm}	Ambient temperature
T_{st}	Temperature of the fuel cell
V_{ca}	Cathode volume
V_{sm}	Supply manifold volume

Manuscript received September 18, 2015; revised January 02, 2016; accepted February 04, 2016. This work was supported in part by the National Natural Science Foundation of China (61525303 and 61503099), the China Postdoctoral Science Foundation funded project (2015M570293) and the Self-Planned Task of State Key Laboratory of Robotics and System (HIT)(201505B). Corresponding author: Jianxing Liu(jx.liu@hit.edu.cn)

J. Liu, W. Luo and L. Wu are with Research Institute of Intelligent Control and Systems, Harbin Institute of Technology, Harbin, 150001, P. R. China.

X. Yang is with Department of Informatics, King's College London, London, WC2R 2LS, United Kingdom.

I. INTRODUCTION

MODERN complex industrial systems can not be operated safely without reliable fault diagnosis and isolation (FDI) schemes in place [1]–[4]. Such systems including PEM fuel cells are vulnerable to system failure or mechanical faults that can lead to catastrophic consequences. Among different kinds of fuel cells, PEM fuel cells are suitable for both stationary and automobile applications due to the ongoing development of PEM technology [5].

One of the main problems in the PEM fuel cell operation is the so-called oxygen starvation phenomenon during fast load variation. Accurate regulation of the oxygen excess ratio is required in order to avoid oxygen starvation [6]. This is a challenging task which comes from two aspects, on one hand, it is difficult to measure the oxygen excess ratio value, on the other hand, the fuel cell systems suffer from various faults, such as sudden air leak in the air supply manifold. Hence, from the point view of fault tolerant control (FTC), only FDI is not enough, the fault signal should be reconstructed and then its effect on the system performance can be compensated during active FTC design.

During the last decades, different kinds of model based techniques have been widely studied in the areas of FDI, health monitoring and complex industrial systems [4], [7]–[13]. Sliding mode based approach is one of the most attractive techniques due to its robustness against external disturbances, high accuracy and fast convergence [14], [15]. Several sliding mode observer (SMO) based FDI approaches have been proposed for linear systems [16], [17], but only few works have been reported for nonlinear systems, especially for nonlinear uncertain systems [15], [18]. However, 1-st order sliding mode algorithms are employed in the above works that require low pass filters to generate the ouput injection signals and induce undesirable chattering effects. Furthermore, the employment of low pass filters will introduce some delays which results in inaccurate estimates or even instability of the sytem. In recent years, higher order sliding mode technique has been widely studied due to the reasons that it does not require any low pass filters while keeping all the good properties of the standard sliding mode [19]–[21]. This technique can also be used to alleviate the chattering effect because of its continuous output signal.

From the application point of view, PEM fuel cell systems have also been the subject of many FDI studies. In [22], a

hydrogen leak detection method based on a control oriented model was developed and the relative humidity sensors were not required. Escobet *et al.* [3] proposed a fault diagnosis methodology based on the PEM fuel cell model including several kinds of faults. The residual signals are computed from the comparisons of measured inputs and outputs. Based on the work [3], a linear parameter varying (LPV) model of the PEM fuel cell system is derived by considering model parameter variation around its operating point, then a linear LPV observer based fault detection approach is implemented to detect several pre-defined fault scenarios [23]. Zhang *et al.* [24] proposed a state space model based fault detection method for a hybrid system which consists of three DC power sources, fuel cells, photovoltaic and batteries. More recently, Dotelli *et al.* [5] proposed a diagnostic approach for detecting PEM fuel cell drying and flooding by analyzing the current ripple generated from the switching power converters. It should be noted that the model used in the above works are obtained from Jacobian linearization approach around pre-defined operating points of the system. However, these operating points are varying according to the operating conditions such as temperature, humidity and air flow rate of the fuel cell power systems [25], [26].

In this paper, a robust fault diagnosis approach based on a modified ST sliding mode algorithm is studied for a class of nonlinear uncertain systems. The modified ST sliding mode algorithm which consists of two nonlinear terms and two linear terms [27], is employed to estimate the system states and reconstruct the fault signal, simultaneously. Then, the fault signal is reconstructed from the equivalent output error injection term calculated on-line from the outputs of the system model and the observer. The time scaling method proposed in [28] is used to determine the error injection term's parameters so that the observer design is considerably simplified. Finally, the proposed fault diagnosis approach is applied to the fuel cell air-feed system. A simplified nonlinear model which sufficiently describes the dynamics of the fuel cell air-feed system, namely, oxygen pressure, total cathode pressure, compressor speed and supply manifold pressure, is used for the observer design [29]. This considered model has been experimentally validated on a 33-kW PEM fuel cell in a wide operating range with less than 5% relative error [30]. A fault scenario, i.e., sudden air leak in the air supply manifold is considered. Its effect is simulated with an increment of supply manifold outlet flow constant, which presents a mechanical failure in the air circuit resulting in an abnormal air flow [3].

The rest of this paper is divided as follows: the model of the PEM fuel cell air-feed system and problem formulation are described in Section II. Section III presents the proposed ST SMO-based FDI approach. In Section IV, the proposed ST SMO-based fault diagnosis method is applied to the PEM fuel cell air feed system, and simulation results are provided to demonstrate the feasibility and effectiveness of the proposed method. Finally, some major conclusions are presented in Section V.

II. Dynamic Modelling of PEM Fuel Cell

A typical PEM fuel cell system is shown in Fig. 1 which consists of four main subsystems, i.e., the air feed subsystem, the hydrogen supply subsystem, the humidify subsystem and the cooling subsystem. In order to achieve high efficient operation, a set of auxiliary elements (valves, compressor, sensors, etc.) are needed to make the fuel cell work at the optimal operating point. In this study, we will focus on the controller design of the air compressor for the air feed subsystem. The air compressor used to supply the oxygen to the cathode side is the core component and can consumes the power generated by the fuel cell up to 30% [31]. Therefore, efficient control of the air compressor is critical for the whole system and effects the system's efficiency directly. A typical PEM fuel cell polarization curve is shown in Fig. 2.

As is widely known, the dynamics of the PEM fuel cell system are with highly nonlinearities. Therefore, suitable control-orient model taking into account the dynamic behaviors of the cathode partial pressure dynamics, the air supply manifold dynamics and the compressor dynamics is needed for the controller design. Some assumptions are made to simplify the nonlinear model of the fuel cell system while keeping the dynamic behaviors of the air-feed subsystem [32]. Mainly, it is assumed that the temperature of the cathode inlet flow is regulated to a constant value through a heat exchanger. This is reasonable because the response time of the stack temperature is slow [33]. The relative humidities of both anode and cathode sides of the fuel cells are regulated to the desired relative humidity through an instantaneous humidifier. The hydrogen pressure in the anode side is regulated to follow the cathode pressure by the anode valve. Only vapor phase is considered inside the cathode and extra water in liquid phase is removed from the channels. The compressor motor current dynamics are neglected because the electrical time constant is very small as compared to the mechanical dynamics [34].

A. Cathode flow model

The thermodynamic properties and mass conservation are used to model the behavior of the air inside the cathode. The dynamics of the oxygen, nitrogen and vapor partial pressures are described by the following equations:

$$\begin{aligned} \frac{dp_{O_2}}{dt} &= \frac{RT_{\text{fc}}}{M_{O_2}V_{\text{ca}}}\left(W_{O_2,\text{in}} - W_{O_2,\text{out}} - W_{O_2,\text{react}}\right), \\ \frac{dp_{N_2}}{dt} &= \frac{RT_{\text{fc}}}{M_{N_2}V_{\text{ca}}}\left(W_{N_2,\text{in}} - W_{N_2,\text{out}}\right), \end{aligned} \tag{1}$$

where T_{fc} is the FC stack temperature, V_{ca} is the lumped volume of cathode and M_{O_2}, M_{N_2} are the molar mass of oxygen and nitrogen, respectively.

The inlet mass flow rates of oxygen and the nitrogen $W_{O_2,\text{in}}, W_{N_2,\text{in}}$ can be calculated from the inlet cathode flow $W_{\text{ca,in}}$,

$$\begin{aligned} W_{O_2,\text{in}} &= x_{O_2}W_{\text{ca,in}}, \\ W_{N_2,\text{in}} &= (1 - x_{O_2})W_{\text{ca,in}}, \end{aligned} \tag{2}$$

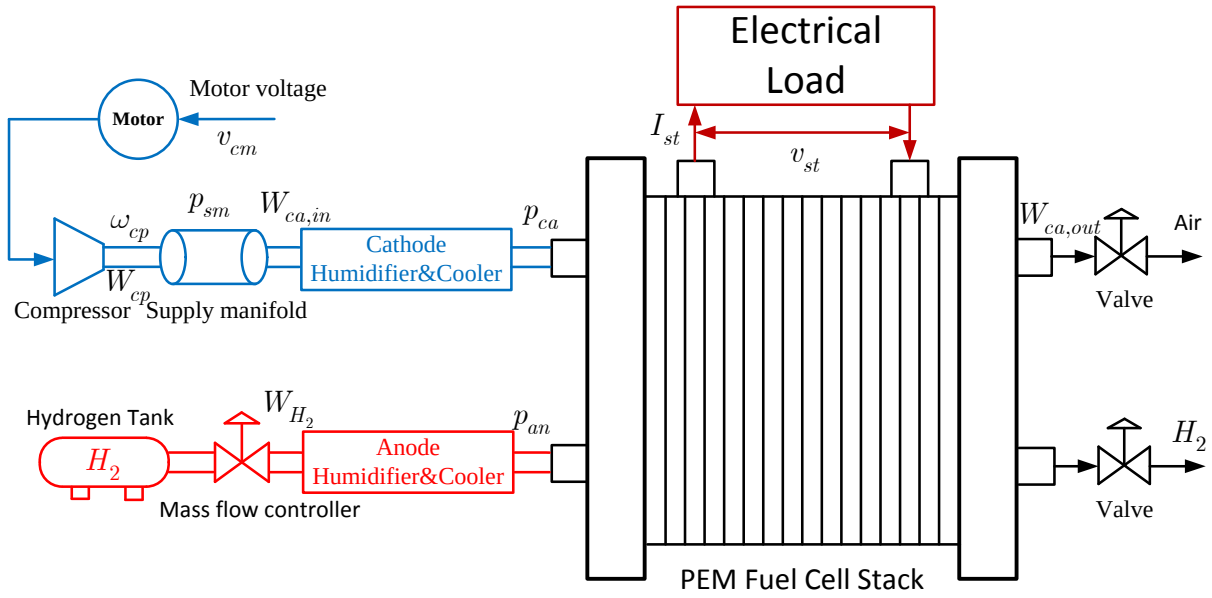

Fig. 1. Fuel cell system scheme

where x_{O_2} is the oxygen mass fraction of the inlet air, and the mass flow rate entering the cathode $W_{\text{ca,in}}$,

$$W_{\text{ca,in}} = \frac{1}{1+\omega_{\text{atm}}} k_{\text{ca,in}}(p_{\text{sm}} - p_{\text{ca}}), \tag{3}$$

where $\omega_{\text{atm}} = \dfrac{M_{\text{v}}}{M_{\text{a,ca,in}}} \dfrac{\phi_{\text{ca}} p_{\text{sat}}(T_{\text{atm}})}{p_{\text{atm}} - \phi_{\text{ca}} p_{\text{sat}}(T_{\text{atm}})}$ is the humidity ratio, $k_{\text{ca,in}}$ is the cathode inlet orifice constant, p_{sm} and $p_{\text{sat}}(T_{\text{atm}})$ are supply manifold pressure and saturation pressure at the atmospheric temperature, respectively. The cathode pressure p_{ca} is assumed to be spatially invariant, which is the sum of oxygen, nitrogen and vapor partial pressures, i.e., $p_{\text{ca}} = p_{O_2} + p_{N_2} + p_{\text{sat}}(T_{\text{fc}})$.

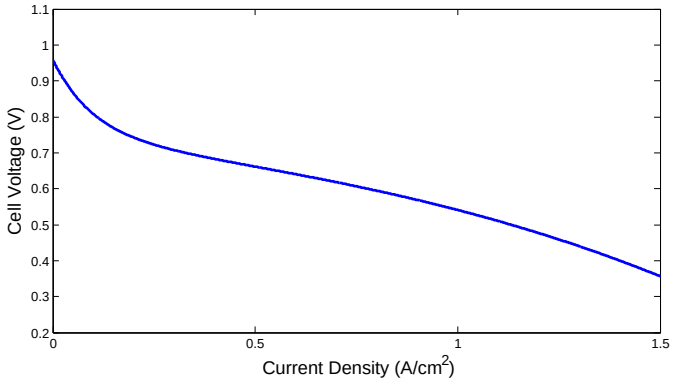

Fig. 2. Typical fuel cell voltage.

The outlet mass flow rates of oxygen and nitrogen $W_{O_2,\text{out}}, W_{N_2,\text{out}}$ are given as:

$$\begin{aligned} W_{O_2,\text{out}} &= \frac{M_{O_2} p_{O_2}}{M_{O_2} p_{O_2} + M_{N_2} p_{N_2} + M_{\text{v}} p_{\text{sat}}} W_{\text{ca,out}}, \\ W_{N_2,\text{out}} &= \frac{M_{N_2} p_{N_2}}{M_{O_2} p_{O_2} + M_{N_2} p_{N_2} + M_{\text{v}} p_{\text{sat}}} W_{\text{ca,out}}, \end{aligned} \tag{4}$$

in which the flow rate at the cathode exit $W_{\text{ca,out}}$ is calculated by the nozzle flow equation proposed in [35],

$$W_{\text{ca,out}} = k_{\text{ca,out}} \sqrt{p_{\text{ca}} - p_{\text{atm}}}. \tag{5}$$

The mass flow rate of oxygen consumption $W_{O_2,\text{react}}$ is expressed as follows:

$$W_{O_2,\text{react}} = \frac{n I_{\text{st}}}{4F} M_{O_2}. \tag{6}$$

B. Air Compressor Model

The air compressor is driven by a torque controlled permanent magnet synchronous motor (PMSM), which provides oxygen to the fuel cell cathode side. The dynamic of the compressor angular velocity ω_{cp} is described by the following equation,

$$\frac{d\omega_{\text{cp}}}{dt} = \frac{1}{J_{\text{cp}}} (\tau_{\text{cm}} - \tau_{\text{cp}}), \tag{7}$$

where τ_{cm} and τ_{cp} are compressor motor torque and load torque, respectively. These two variables are calculated as follows:

$$\begin{aligned} \tau_{\text{cm}} &= \eta_{\text{cm}} \frac{k_t}{R_{\text{cm}}} (v_{\text{cm}} - k_v \omega_{\text{cp}}), \\ \tau_{\text{cp}} &= \frac{C_p}{\omega_{\text{cp}}} \frac{T_{\text{atm}}}{\eta_{\text{cp}}} \left[\left(\frac{p_{\text{sm}}}{p_{\text{atm}}} \right)^{\frac{\gamma-1}{\gamma}} - 1 \right] W_{\text{cp}}, \end{aligned} \tag{8}$$

where v_{cm} is the compressor motor input voltage, k_t, R_{cm}, k_v are motor constants and W_{cp} is the compressor flow rate.

C. Supply Manifold Model

The supply manifold model is described by the following equation

$$\frac{dp_{\text{sm}}}{dt} = \frac{R_{\text{a}} T_{\text{cp,out}}}{V_{\text{sm}}} (W_{\text{cp}} - W_{\text{sm,out}}), \tag{9}$$

where $T_{\text{cp,out}}$ is the compressor's air temperature and is calculated as follows:

$$T_{\text{cp,out}} = T_{\text{atm}} + \frac{T_{\text{atm}}}{\eta_{\text{cp}}}\left[\left(\frac{p_{\text{sm}}}{p_{\text{atm}}}\right)^{\frac{\gamma-1}{\gamma}} - 1\right], \quad (10)$$

where η_{cp} is the compressor efficiency (its maximum value is 80%).

Due to the small pressure difference between the supply manifold p_{sm} and the cathode p_{ca}, a linear nozzle equation is given as follows:

$$W_{\text{sm,out}} = k_{\text{sm,out}}\left(p_{\text{sm}} - p_{\text{ca}}\right). \quad (11)$$

D. State Space Representation

In view of Eqs. (1-11) and define the state variables $x = [x_1,\ x_2,\ x_3,\ x_4]^T = [p_{O_2},\ p_{N_2},\ \omega_{\text{cp}},\ p_{\text{sm}}]^T$. Then, the nonlinear dynamics of the fuel cell air-feed system are expressed by the following equations:

$$\dot{x} = F(x) + G \cdot u + \Psi \cdot \xi, \quad (12)$$

where

$$F(x) = \begin{pmatrix} b_1(x_4 - X) - x_1 f_1(x_1, x_2) \\ b_1(x_4 - X) - x_2 f_1(x_1, x_2) \\ -c_9 x_3 - \dfrac{b_{10}}{x_3}\left[\left(\dfrac{x_4}{b_{11}}\right)^{b_{12}} - 1\right] f_2(x_3, x_4) \\ f_3(x_4) \times \left[f_2(x_3, x_4) - b_{16}\left(x_4 - X\right)\right] \end{pmatrix},$$

$$G = \begin{pmatrix} 0 \\ 0 \\ b_{13} \\ 0 \end{pmatrix}, \quad \Psi = \begin{pmatrix} -b_7 \\ 0 \\ 0 \\ 0 \end{pmatrix},$$

in which $X = x_1 + x_2 + b_2$, $f_1(x_1, x_2) := \dfrac{b_3}{b_4 x_1 + b_5 x_2 + b_6} W_{\text{ca,out}}$, $f_2(x_3, x_4) := W_{\text{cp}}$ and $f_3(x_4) := b_{14}\left(1 + b_{15}\left[\left(\dfrac{x_4}{b_{11}}\right)^{b_{12}} - 1\right]\right)$. The stack current $\xi := I_{\text{st}}$ is considered as the external disturbance and the control input $u := v_{\text{cm}}$ is the motor's input voltage. The outputs and performance variables of the system are given by:

$$\begin{aligned} y &= \begin{bmatrix} y_1 & y_2 & y_3 \end{bmatrix}^T = \begin{bmatrix} p_{\text{sm}} & W_{\text{cp}} & V_{\text{st}} \end{bmatrix}^T, \\ z &= \begin{bmatrix} z_1 & z_2 \end{bmatrix}^T = \begin{bmatrix} P_{\text{net}} & \lambda_{O_2} \end{bmatrix}^T, \end{aligned} \quad (13)$$

where P_{net} and λ_{O_2} are fuel cell net power and oxygen excess ratio, respectively.

The fuel cell net power P_{net} is the difference between the power produced by the stack P_{st} and the power consumed by the compressor. Thus, the net power can be expressed as:

$$P_{\text{net}} = P_{\text{st}} - P_{\text{cp}}, \quad (14)$$

where $P_{\text{st}} = I_{\text{st}} V_{\text{st}}$ and $P_{\text{cp}} = \tau_{\text{cm}} \omega_{\text{cp}}$ are the stack power and compressor power, respectively. The oxygen excess ratio λ_{O_2} is defined by the following equation:

$$\lambda_{O_2} = \frac{W_{O_2,\text{in}}}{W_{O_2,\text{react}}} = \frac{b_{16}\left(p_{\text{sm}} - p_{\text{ca}}\right)}{b_{17} I_{\text{st}}}. \quad (15)$$

The parameters $b_i,\ \ i \in \{1, \cdots, 17\}$ are defined in Appendix A1. More details on this model are available in [6], [29].

Remark 1: As is well known that a set of auxiliary are needed to make the fuel cell work at its optimal operating conditions. Particularly, due to it is essential to regulate the oxygen excess ratio close to 2 in the presence of fast load variation and fault scenario [36], [37]. The level of λ_{O_2} is critical because fast load demand will result sudden decrease of the oxygen flow rate. On one hand, once the value of oxygen excess ratio decreases to a critical value (normally less than 1), oxygen starvation phenomenon which leads to the FC degradation occurs. On the other hand, higher value improves the fuel cell stack power but also result in higher power consumption of the air compressor. Therefore, the problems of oxygen excess ratio estimation and fault reconstruction arise due to the reasons of safety and high efficiency.

In the following section, we will design an ST SMO based FDI approach for the fuel cell air-feed system using the information of the system outputs. Then, based on the proposed ST SMO, the fault signal is reconstructed via equivalent output error injection method.

III. ST SMO-Based FDI Design

A. ST SMO Design

Consider a nonlinear system given as follows:

$$\begin{aligned} \dot{z} &= Az + g(z, u) + D(y, u) f(t), \\ y &= Cz, \end{aligned} \quad (16)$$

where $z = [z_1, z_2]^T \in \mathbb{R}^n,\ z_1 \in \mathbb{R}^p,\ z_2 \in \mathbb{R}^{n-p}$, is the system state vector, $u(t) \in \mathcal{U} \subset \mathbb{R}^m$ is the system input which is assumed to be known, $y \in \mathcal{Y} \subset \mathbb{R}^p$ is the output vector. $A = \begin{bmatrix} A_1^{p\times p} & A_2^{(p-1)\times(p-1)} \\ A_3^{p\times p} & A_4^{(p-1)\times(p-1)} \end{bmatrix} \in \mathbb{R}^{n\times n}$ in which A_4 is Hurwitz stable and $C \in \mathbb{R}^{p\times n}$ are constant matrices with C of full rank $(q \le p < n)$. The known nonlinear function $g(z, u) \in \mathbb{R}^n$ is Lipschitz with respect to z uniformly for $u \in \mathcal{U}$, $D(y, u) \in \mathbb{R}^{n\times q}$ is assumed to be a smooth and bounded function depending on the system inputs and outputs. The smooth fault signal vector $f(t) \in \mathbb{R}^q$ satisfies

$$\|f(t)\| \le \rho_1, \quad \left\|\dot{f}(t)\right\| \le \rho_2, \quad (17)$$

where the positive constants ρ_1 and ρ_2 are known.

By reordering the state variables, (16) can be rewritten as

$$\begin{aligned} \dot{z}_1 &= A_1 z_1 + A_2 z_2 + g_1(z, u) + D_1(y, u) f(t), \\ \dot{z}_2 &= A_3 z_1 + A_4 z_2 + g_2(z, u), \\ y &= z_1, \end{aligned} \quad (18)$$

where $g(z, u) = \begin{bmatrix} g_1(z, u) \\ g_2(z, u) \end{bmatrix}$, $D(y, u) = \begin{bmatrix} D_1(y, u) \\ 0 \end{bmatrix}$ and $D(y, u)_1$ is a bounded nonsingular matrix in $(y, u) \in \mathcal{Y} \times \mathcal{U}$

Assumption 1: The known nonlinear terms $g_1(z, u)$ and $g_1(z, u)$ are Lipschitz continuous with respect to z_2, i.e.,

$$\|g_i(z_1, z_2, u) - g_i(z_1, \hat{z}_2, u)\| \le \gamma_i \|z_2 - \hat{z}_2\|, \quad (19)$$

where $\gamma_i,\ i \in \{1, 2\}$ are known positive constants [38].

Consider the system (18), a ST SMO is designed as follows:

$$\begin{aligned}\dot{\hat{z}}_1 &= A_1 y + A_2\hat{z}_2 + g_1(\hat{z},u) + \upsilon(y-\hat{y}),\\ \dot{\hat{z}}_2 &= A_3 y + A_4\hat{z}_2 + g_2(\hat{z},u),\\ \hat{y} &= \hat{z}_1,\end{aligned} \tag{20}$$

where $\upsilon(\cdot)$ is the output error injection term generated by the modified ST algorithm [19]:

$$\begin{aligned}\upsilon(s) &= k_1|s|^{\frac{1}{2}}\text{sign}(s) + k_2\int_0^t \text{sign}(s)d\tau\\ &\quad + k_3 s + k_4\int_0^t s d\tau,\end{aligned} \tag{21}$$

where $k_i,\ i\in\{1,2,3,4\}$ are positive constants to be determined.

Denote $e_y = y-\hat{y}$ and $e_2 = z_2 - \hat{z}_2$, subtract (20) from (18), the error dynamical system is given by:

$$\dot{e}_y = -\upsilon(e_y) + A_2 e_2 + \Delta g_1 + D_1(y,u)f(t), \tag{22}$$

$$\dot{e}_2 = A_4 e_2 + \Delta g_2, \tag{23}$$

where $\Delta g_1 = g_1(z,u) - g_1(\hat{z},u)$ and $\Delta g_2 = g_2(z,u) - g_2(\hat{z},u)$.

Proposition 1: Suppose that Assumption 1 holds, the error dynamical system (23) is exponential stable if there exists a positive definite matrix Ψ, which satisfies the following inequality

$$A_4^T\Psi + \Psi A_4 + \frac{1}{\varepsilon}\Psi\Psi^T + \varepsilon\gamma_2^2 I_{n-p} + \sigma I_{n-p} < 0, \tag{24}$$

where ε and σ are two small positive constants.

Proof: Consider a Lyapunov candidate function $W = e_2^T\Psi e_2$, its first time derivative is calculated as follows:

$$\begin{aligned}\dot{W} &= e_2^T(A_4^T\Psi + \Psi A_4)e_2 + 2e_2^T\Psi\Delta g_2\\ &\le e_2^T(A_4^T\Psi + \Psi A_4)e_2 + \frac{1}{\varepsilon}e_2^T\Psi\Psi^T e_2 + \varepsilon\gamma_2^2\|e_2\|^2\\ &\le e_2^T\left(A_4^T\Psi + \Psi A_4 + \frac{1}{\varepsilon}\Psi\Psi^T + \varepsilon\gamma_2^2 I_{n-p}\right)e_2\\ &< -\sigma e_2^T e_2 \le -\frac{\sigma}{\lambda_{\min}(\Psi)}W.\end{aligned} \tag{25}$$

Hence, the conclusion can be directly obtained from (25), i.e., $\lim_{t\to\infty} e_2(t) = 0$. ∎

In view of (23), we can conclude from the results of Proposition 1 that $\dot{e}_2$ is bounded. Under the conditions (17) and (19), the time derivative of the nonlinear term in (22) $A_2e_2 + \Delta g_1 + D_1(y,u)f(t)$ is bounded:

$$\left\|\phi(t) = \frac{d}{dt}\left(A_2e_2 + \Delta g_1 + D_1(y,u)f(t)\right)\right\| \le \delta, \tag{26}$$

where δ is a positive constant.

Theorem 1: Suppose that (26) holds, the trajectories of the error dynamical system (22) converges to zero in finite time if the designing gains k_i in the modified ST algorithm (21) are formulated as

$$\begin{aligned}k_1 &= k_{10}\sqrt{L},\quad k_2 = k_{20}L,\\ k_3 &= k_{30}L,\quad k_4 = k_{40}L^2,\end{aligned} \tag{27}$$

where $k_{i0},\ i\in\{1,2,3,4\}$ and L are positive constants which satisfy

$$4k_{20}k_{40} > 8k_{30}^2k_{20} + 9k_{10}^2k_{30}^2, \tag{28}$$

$$L > \frac{\delta\|q_1\|_2}{\sqrt{\lambda_{\min}(P)}}\frac{\sqrt{\lambda_{\max}(P)}}{\lambda_{\min}(M_1)}. \tag{29}$$

Proof: The system (22) can be rewritten as

$$\begin{aligned}\dot{e}_y &= -k_1|e_y|^{\frac{1}{2}}\text{sign}(e_y) - k_3 e_y + \varepsilon,\\ \dot{\varepsilon} &= -k_2\text{sign}(e_y) - k_4 e_y + \phi(t).\end{aligned} \tag{30}$$

In order to perform Lyapunov analysis, the following state vector is introduced

$$\xi = \left[L^{\frac{1}{2}}|e_y|^{\frac{1}{2}}\text{sign}(e_y), Le_y, \varepsilon\right]^T. \tag{31}$$

The system (30) is rewritten as

$$\dot{\xi} = \frac{L}{|\xi_1|}F_1\xi + LF_2\xi + F_3, \tag{32}$$

where $F_1 = \begin{bmatrix}-\frac{\lambda_0}{2} & 0 & \frac{1}{2}\\ 0 & -\lambda_0 & 0\\ -\alpha_0 & 0 & 0\end{bmatrix}$, $F_2 = \begin{bmatrix}-\frac{k_{\lambda_0}}{2} & 0 & 0\\ 0 & -k_{\lambda_0} & 1\\ 0 & -k_{\alpha_0} & 0\end{bmatrix}$ and $F_3 = \begin{bmatrix}0 & 0 & \phi(t)\end{bmatrix}^T$. The following candidate Lyapunov function is chosen for the system (32)

$$V = \xi^T P\xi, \tag{33}$$

where the matrix $P = \frac{1}{2}\begin{bmatrix}4k_{20}+k_{10}^2 & k_{10}k_{30} & -k_{10}\\ k_{10}k_{30} & k_{30}^2+2k_{40} & -k_{30}\\ -k_{10} & -k_{30} & 2\end{bmatrix}$ is symmetric positive definite due to the fact that its leading principle minors are all positive given that $4k_{20}k_{40} > 8k_{10}^2k_{20} + 9k_{10}^2k_{30}^2$.

Taking the time derivative of (33) along the trajectories of (32),

$$\dot{V} = -\frac{L}{|\xi_1|}\xi^T M_1\xi - L\xi^T M_2\xi + q_1\phi(t)\xi, \tag{34}$$

where $q_1 = \begin{bmatrix}-\lambda_0 & -k_{\lambda_0} & 2\end{bmatrix}$, $M_1 = F_1^TP + PF_1$ and $M_2 = F_2^TP + PF_2$ are positive definite matrices under the condition (28).

It follows from the inequality $\lambda_{\min}(P)\|\xi\|^2 \le V \le \lambda_{\max}(P)\|\xi\|^2$ that

$$\begin{aligned}\dot{V} &\le -L\frac{\lambda_{\min}(M_1)}{\sqrt{\lambda_{\max}(P)}}V^{\frac{1}{2}} - L\frac{\lambda_{\min}(M_2)}{\lambda_{\max}(P)}V + \frac{\delta\|q_1\|_2}{\sqrt{\lambda_{\min}(P)}}V^{\frac{1}{2}},\\ &= -\left(L\frac{\lambda_{\min}(M_1)}{\sqrt{\lambda_{\max}(P)}} - \frac{\delta\|q_1\|_2}{\sqrt{\lambda_{\min}(P)}}\right)V^{\frac{1}{2}} - L\frac{\lambda_{\min}(M_2)}{\lambda_{\max}(P)}V\\ &\le -\eta V^{\frac{1}{2}},\end{aligned} \tag{35}$$

where $\eta = L\frac{\lambda_{\min}(M_1)}{\sqrt{\lambda_{\max}(P)}} - \frac{\delta\|q_1\|_2}{\sqrt{\lambda_{\min}(P)}}$ is a positive constant according to the condition (29). Therefore, it follows that the comparison principle that ξ converge to zero in finite time [39]. Thus, Theorem 1 is proven. ∎

B. Fault Reconstruction

In this part, a ST SMO based fault reconstruction approach will be designed for the system (16) via equivalent output error injection technique [16]. Theorem 1 shows that e_y and $\dot{e}_y$ converge to zero in finite time, thus, the following equation is obtained during the sliding motion $e_y = \dot{e}_y = 0$

$$\upsilon(e_y) \;=\; A_2 e_2 + \Delta g_1 + D_1(y,u) f(t). \tag{36}$$

According to the results of Proposition 1, we have

$$\lim_{t\to\infty} \|A_2 e_2 + \Delta g_1\| \le (\|A_2\| + \gamma_1)\, \|e_2(t)\| = 0. \tag{37}$$

Therefore, provided that the matrix $D_1(y,u)$ is invertible, the fault signal $f(t)$ can be approximated by

$$\hat{f}(t) \;=\; D_1^{-1}(y,u)\upsilon(e_{y_2}). \tag{38}$$

Remark 2: It should be pointed out that the calculations required for the modified ST algorithm (21) are slightly more intensive than those of the proportional integral (PI) algorithm. However, from the practical point of view, the correction term $\upsilon(s)$ entails low real-time computational burden due to high computational capabilities of digital computers.

IV. Simulation Results

The proposed ST SMO-based FDI approach has been implemented on the Matlab/Simulink environment. The physical system parameters used in simulation test are given in Table I.

TABLE I
PHYSICAL PARAMETERS OF THE SYSTEM

Symbol	Parameter	Value
n	Number of cells in stack	90
γ	Ratio of specific heats of air	1.4
$\phi_{\rm ca}$	Relative humidity in cathode inlet	1.0
$\phi_{\rm atm}$	Relative humidity in ambient air	0.5
R	Universal gas constant	8.314 J/(mol·K)
F	Faraday constant	96485 C/mol
$p_{\rm atm}$	Atmospheric pressure	1.01325 $\times 10^5$ Pa
$T_{\rm fc}$	Temperature of the fuel cell	353.15 K
$T_{\rm atm}$	Atmospheric temperature	298.15 K
C_p	Specific heat capacity of air	1004 J/(Kg·K)
C_D	Discharge of the nozzle	0.0124
$y_{O_2,\rm atm}$	Oxygen molar ratio at cathode inlet	0.21
M_a	Air molar mass	28.9644$\times 10^{-3}$ Kg/mol
M_{O_2}	Oxygen molar mass	32$\times 10^{-3}$ Kg/mol
M_{N_2}	Nitrogen molar mass	28$\times 10^{-3}$ Kg/mol
M_v	Vapor molar mass	18$\times 10^{-3}$ Kg/mol
$V_{\rm ca}$	Cathode volume	0.01 m^3
$V_{\rm sm}$	Supply manifold volume	0.02 m^3
A_T	Opening area of the nozzle	0.002 m^2
$J_{\rm cp}$	Compressor and motor inertia	5×10^{-5} Kg·m^2
$\eta_{\rm cp}$	Compressor efficiency	80%
$\eta_{\rm cm}$	Motor mechanical efficiency	98%
k_t	Motor constant	0.0153 N·m/A
k_v	Motor constant	0.0153 V/(rad/sec)
$R_{\rm cm}$	Motor constant	0.82 Ω
$k_{\rm sm,out}$	Supply manifold outlet constant	0.3629$\times 10^{-5}$ Kg/(Pa·s)
$k_{\rm ca,in}$	Cathode inlet constant	0.3629$\times 10^{-5}$ Kg/(Pa·s)
$k_{\rm ca,out}$	Cathode outlet constant	0.2177$\times 10^{-5}$ Kg/(Pa s)

Assumption 2: Suppose that the following equation

$$c_4 x_1 + c_5 x_2 + c_2 \;=\; \kappa X, \tag{39}$$

holds in the operation domain for some positive constant κ. Fig. 3 shows the exact value of κ and its constant approximation value [30], [40].

Under the Assumption 2, the model of the feul cell air feed system (12) can be rewritten as follows:

$$\begin{bmatrix} \dot{X} \\ \dot{x}_2 \\ \dot{x}_3 \\ \dot{x}_4 \end{bmatrix} = \begin{bmatrix} b_1(x_4 - X) - (X - b_2) f_1(X) - b_1 \xi \\ b_1(x_4 - X) - x_2 f_1(X) \\ -c_9 x_3 - f_4(x_3, x_4) + b_{13} u \\ f_3(x_4) \times [f_2(x_3, x_4) - b_{16}\,(x_4 - X)] \end{bmatrix}, \tag{40}$$

where $f_4(x_3, x_4) = \dfrac{b_{10}}{x_3}\left[\left(\dfrac{x_4}{b_{11}}\right)^{b_{12}} - 1\right] f_2(x_3, x_4)$.

A. Model validation

The fuel cell stack model is obtained from a single-cell static characteristic [41]. The stack output voltage $V_{\rm st}$ is calculated as follows

$$V_{\rm st} = n\left(E - v_{\rm act} - v_{\rm ohm} - v_{\rm conc}\right), \tag{41}$$

where E is the open circuit voltage, $v_{\rm act}$, $v_{\rm ohm}$ and $v_{\rm conc}$ are the losses of activation, ohmic and concentration, respectively. Those losses are strongly linked to the current density and can be calculated as follows

$$\begin{aligned} v_{\rm act} &= v_0 + v_a\left(1 - e^{-b_1 i}\right), \\ v_{\rm ohm} &= i R_{\rm ohm}, \quad v_{\rm conc} = i\left(b_3 \frac{i}{i_{\rm max}}\right)^{b_4}, \end{aligned} \tag{42}$$

where i is the current density, $A_{\rm fc}$ is the active area, v_0 is the voltage drop at zero current density, b_3, b_4 and $i_{\rm max}$, v_a and b_1 are positive constants and $R_{\rm ohm}$ is the fuel cell internal electrical resistance [33].

The stack voltages obtained from the 4-th order model (40) and the 9-th order model [6] are shown and compared in Fig. 4. In view of Fig. 4, it can be seen that the output stack voltage computed from the 4-th order model is very close to that from the 9-th order model, i.e, with relative error less than 2.5%. Thus, we can conclude that the performance of the 4-th order model replicates the dynamics of the 9-th order model with sufficient precision.

For the simulation purpose, the initial errors of the states are set at 20% of maximum deviation from the 9-th order model. The initial values were chosen as

$$\begin{aligned} \hat{p}_{O_2} &= 0.09 \text{ bar}, \quad \hat{p}_{N_2} = 0.7 \text{ bar}, \\ \hat{\omega}_{\rm cp} &= 750 \text{ RPM}, \quad \hat{p}_{\rm sm} = 1.1 \text{ bar}. \end{aligned} \tag{43}$$

During the simulation tests, the stack current was varied between 100 A and 300 A in order to demonstrate the fuel cell model characteristics, as shown in Fig. 5. A static feed-forward controller is used to control the compressor voltage so that the oxygen excess ratio level is close to 2. It can be seen from the Fig. 5 that a step load increase (i.e. $t = 20$ sec) causes a sudden drop in the oxygen excess ratio. The performance variables ($P_{\rm net}$, λ_{O_2}) in Fig. 6 and the states variables (p_{O_2}, p_{N_2}, $\omega_{\rm cp}$, $p_{\rm sm}$) in Figs. 7 and 8 show that the four states model matches well with the 9-th order model's outputs.

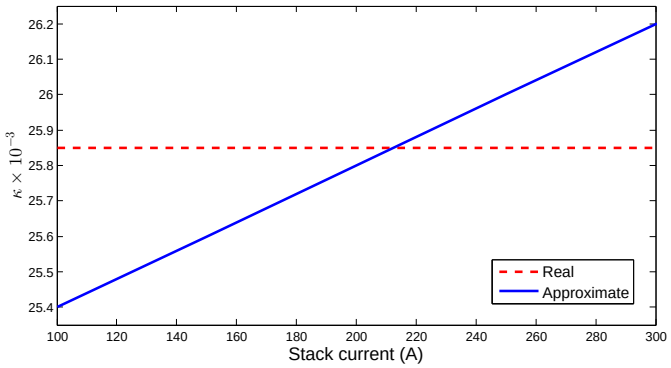

Fig. 3. Approximation of parameter κ with respect to stack current

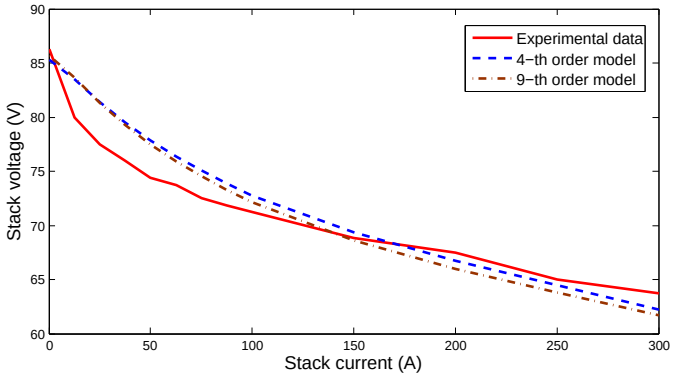

Fig. 4. Stack voltage response.

B. Fault scenario

The fault scenario of a sudden air leak in the air supply manifold is considered, which is simulated with a parameter increment Δc_{16} in the supply manifold outlet flow constant $c_{16} := k_{\text{sm,out}}$. This effect is translated into a change in the outlet air flow in the supply manifold: $W_{\text{sm,out}} = (c_{16} + \Delta c_{16})(x_4 - x_1)$ [3], [12], [23]. The fault signal $f(t)$ is given as

$$f(t) = \begin{cases} \Delta c_{16_1} \times (x_4 - x_1), & \text{if t} \in [30, 60) \\ \Delta c_{16_2} \times (x_4 - x_1), & \text{if t} \in [60, 90) \\ 0, & \text{else} \end{cases} \quad (44)$$

in which $\Delta c_{16_1} = 0.2 c_{16}$ and $\Delta c_{16_2} = 1.0 c_{16}$.

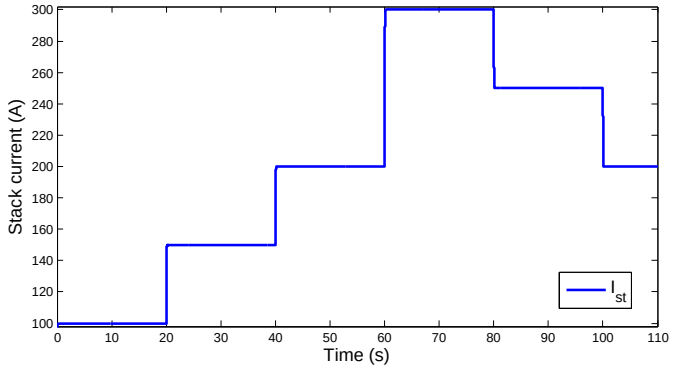

Fig. 5. Stack current under load variation

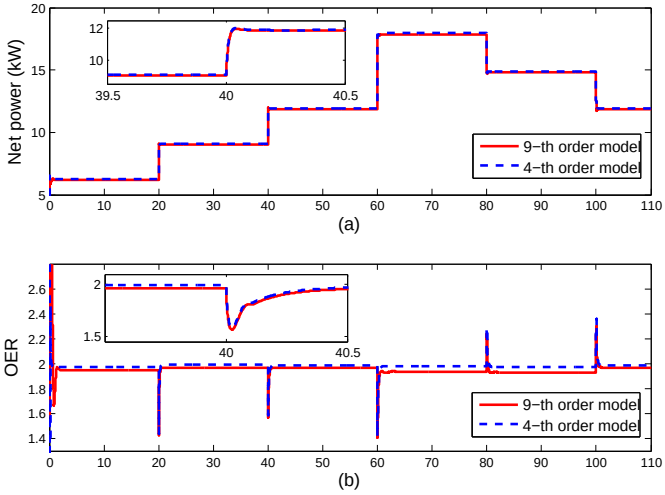

Fig. 6. Performance comparisons of (a) P_{net} and (b) λ_{O_2}.

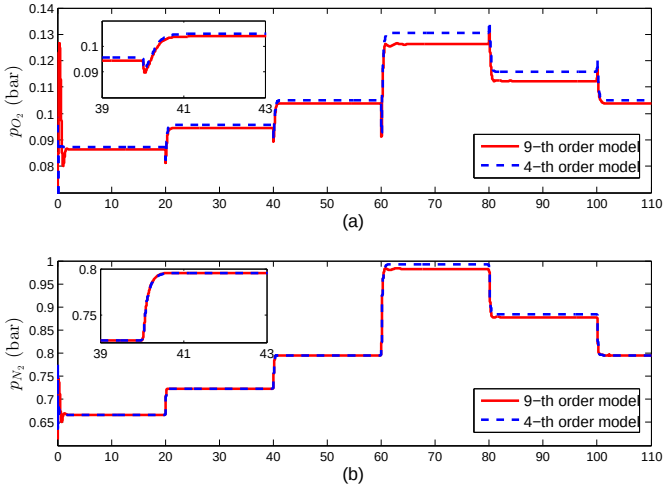

Fig. 7. Performance comparisons of (a) p_{O_2} and (b) p_{N_2}.

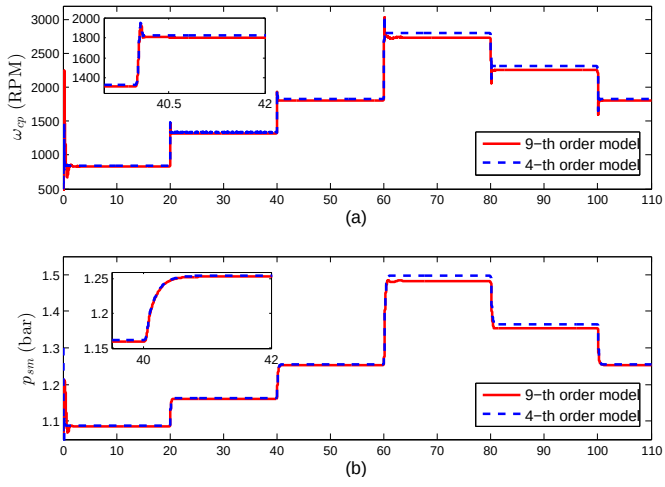

Fig. 8. Performance comparisons of (a) ω_{cp} and (b) p_{sm}.

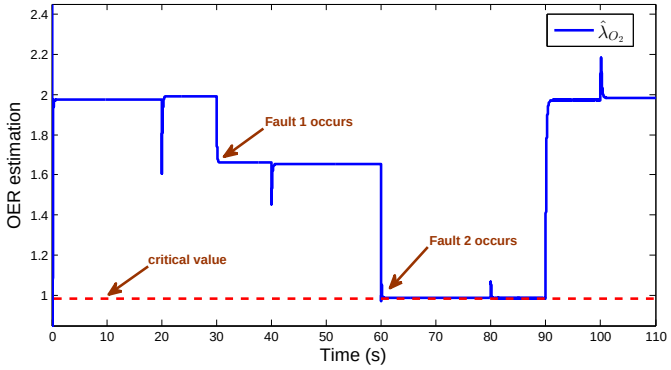

Fig. 9. Estimate of oxygen excess ratio.

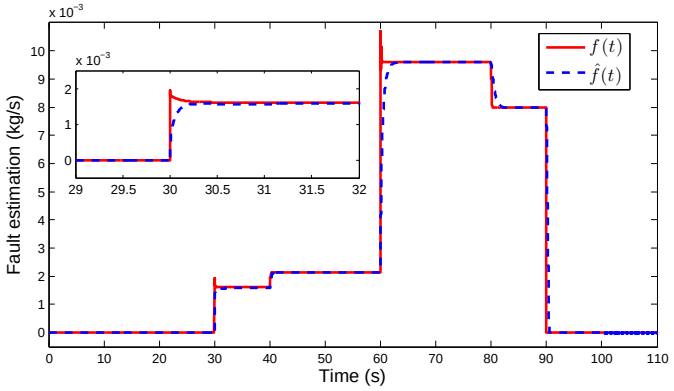

Fig. 10. Estimate of fault signal.

Based on the proposed ST SMO, oxygen excess ratio is estimated via the system outputs (cathode pressure, supply manifold pressure, output stack voltage), as shown in Fig. 9. It is easy to find that this value decreases at $t = 30$ sec and $t = 60$ sec, respectively. It happens because of the fault occurrence at that time instant, which results in decrease of the oxygen flow rate supplied to the cathode. Taking into account the effect of the fault, the air compressor needs to increase the air flow supply, in order to ensure the fuel cell's safe operation. It should be noted that at time $t = 60$ sec, the oxygen excess ratio is less than its critical value (normally 1), which indicates that the oxygen starvation phenomenon occurs. In this case, the fuel cell should be shut off immediately to protect the fuel cell. Based on the equivalent output error injection technique, this fault signal is reconstructed faithfully as shown in Fig. 10. It is clear that the proposed scheme is capable of reconstructing fault signal and state estimation simultaneously in the presence of load variation.

V. CONCLUSIONS

This paper has proposed a robust fault diagnosis method for the PEM feul cell air-feed system. The residual signals are generated by comparing the output variables of the fuel cell air feed system model and its corresponding estimate provided by observers. The proposed observer design is based on the modified ST sliding mode algorithm which consists of two nonlinear terms and two linear terms. This observer is able to estimate not only the system states but also fault signals, in the presence of external disturbances. Once the sliding motion is achieved, the obtained equivalent output error injection was computed online to reconstruct the possible faults in the system. The proposed fault diagnosis approach was successfully implemented on Matlab/Simulink environment, where sudden air leak in the air supply manifold is considered as the fault scenario. We have found that when the magnitude of the fault signal increases to a certain value, the oxygen excess ratio will decrease to its critical value, which means that the oxygen starvation phenomenon occurs inside the fuel fell stack. Thus, the air flow supplied by the air compressor needs to increase in order to increase the supply of oxygen flow rate, or even the FC stack should be shut off immediately.

APPENDIX

$$b_1 = \frac{RT_{\text{fc}}k_{\text{ca,in}}}{M_{O_2}V_{\text{ca}}}\frac{x_{O_2,\text{atm}}}{1+\omega_{\text{atm}}}, \quad b_2 = p_{\text{sat}}$$

$$b_3 = \frac{RT_{\text{fc}}}{V_{\text{ca}}}, \quad b_4 = M_{O_2}$$

$$b_5 = M_{N_2}, \quad b_6 = M_{\text{v,ca}}$$

$$b_7 = \frac{nRT_{\text{fc}}}{4FV_{\text{ca}}}, \quad b_8 = \frac{RT_{\text{fc}}k_{\text{ca,in}}}{M_{N_2}V_{\text{ca}}}\frac{1-x_{O_2,\text{atm}}}{1+\omega_{\text{atm}}}$$

$$b_9 = \frac{k_v k_t \eta_{\text{cm}}}{J_{\text{cp}}R_{\text{cm}}}, \quad b_{10} = \frac{C_p T_{\text{atm}}}{J_{\text{cp}}\eta_{\text{cp}}}$$

$$b_{11} = p_{\text{atm}}, \quad b_{12} = \frac{\gamma-1}{\gamma}$$

$$b_{13} = \frac{\eta_{\text{cm}}k_t}{J_{\text{cp}}R_{\text{cm}}}, \quad b_{14} = \frac{\gamma RT_{\text{atm}}}{M_a V_{\text{sm}}}$$

$$b_{15} = \frac{1}{\eta_{\text{cp}}}, \quad b_{16} = k_{\text{ca,in}}\frac{x_{O_2,\text{atm}}}{1+\omega_{\text{atm}}}$$

$$b_{17} = \frac{nM_{O_2}}{4F}.$$

REFERENCES

[1] Y. Zhang and J. Jiang, "Bibliographical review on reconfigurable fault-tolerant control systems," *Annual Reviews in Control*, vol. 32, no. 2, pp. 229–252, 2008.

[2] S. Yin, G. Wang, and H. Gao, "Data-driven process monitoring based on modified orthogonal projections to latent structures," *IEEE Trans. Control Syst. Technol.*, vol. PP, no. 99, pp. 1–8, 2015.

[3] T. Escobet, D. Feroldi, S. D. Lira, V. Puig, J. Quevedo, J. Riera, and M. Serra, "Model-based fault diagnosis in pem fuel cell systems," *J Power Sources*, vol. 192, no. 1, pp. 216–223, 2009.

[4] E. Romero-Cadaval, G. Spagnuolo, L. G. Franquelo, C.-A. Ramos-Paja, T. Suntio, and W.-M. Xiao, "Grid-connected photovoltaic generation plants components and operation," *IEEE Ind. Electron. Mag.*, vol. 7, no. 3, pp. 6–20, Sep 2013.

[5] G. Dotelli, R. Ferrero, P. G. Stampino, S. Latorrata, and S. Toscani, "Diagnosis of pem fuel cell drying and flooding based on power converter ripple," *IEEE Trans. Instrum. Meas.*, vol. 63, no. 10, pp. 2341–2348, 2014.

[6] J. Pukrushpan, A. Stefanopoulou, and H. Peng, "Control of fuel cell breathing: initial results on the oxygen starvation problem," *IEEE Control Syst. Mag.*, vol. 24, no. 2, pp. 30–46, 2004.

[7] S. Vazquez, J. A. Sanchez, J. M. Carrasco, J. I. Leon, and E. Galvan, "A model-based direct power control for three-phase power converters," *IEEE Trans. Ind. Electron.*, vol. 55, no. 4, pp. 1647–1657, April 2008.

[8] J. Pak, C. Ahn, Y. Shmaliy, P. Shi, and M. Lim, "Switching extensible FIR filter bank for adaptive horizon state estimation with application," *IEEE Trans. Control Syst. Technol.*, vol. 99, pp. 1–1, 2015.

[9] C. K. Ahn, P. Shi, and M. Basin, "Two-dimensional dissipative control and filtering for roesser model," *IEEE Trans. Autom. Control*, vol. 60, no. 7, pp. 1745–1759, July 2015.

[10] J. M. Pak, C. K. Ahn, Y. Shmaliy, and M. T. Lim, "Improving reliability of particle filter-based localization in wireless sensor networks via hybrid particle/FIR filtering," *IEEE Trans. Ind. Informat.*, vol. 11, no. 5, pp. 1089–1098, 2015.
[11] X. Su, P. Shi, L. Wu, and Y.-D. Song, "Fault detection filtering for nonlinear switched stochastic systems," *IEEE Trans. Autom. Control*, vol. 99, pp. 1–8, 2015, early Access.
[12] S. Laghrouche, J. Liu, F.-S. Ahmed, M. Harmouche, and M. Wack, "Adaptive second-order sliding mode observer-based fault reconstruction for PEM fuel cell air-feed system," *IEEE Trans. Control Syst. Technol.*, vol. 23, no. 3, pp. 1098–1109, May 2015.
[13] J. Napoles, A. J. Watson, J. J. Padilla, J. I. Leon, L. G. Franquelo, P. W. Wheeler, and M. A. Aguirre, "Selective harmonic mitigation technique for cascaded h-bridge converters with nonequal dc link voltages," *IEEE Trans. Ind. Electron.*, vol. 60, no. 5, pp. 1963–1971, May 2013.
[14] A. Levant, "Sliding order and sliding accuracy in sliding mode control," *International Journal of Control*, vol. 58, no. 6, pp. 1247–1263, 1993.
[15] L. Fridman, Y. Shtessel, C. Edwards, and X.-G. Yan, "Higher-order sliding-mode observer for state estimation and input reconstruction in nonlinear systems," *International Journal of Robust and Nonlinear Control*, vol. 18, no. 4-5, pp. 399–412, 2008.
[16] C. Edwards, S. Spurgeon, and R. Patton, "Sliding mode observers for fault detection and isolation," *Automatica*, vol. 36, no. 4, pp. 541–553, 2000.
[17] C. Tan and C. Edwards, "Sliding mode observers for robust detection and reconstruction of actuator and sensor faults," *International Journal of Robust and Nonlinear Control*, vol. 13, no. 5, pp. 443–463, 2003.
[18] X.-G. Yan and C. Edwards, "Adaptive sliding-mode-observer-based fault reconstruction for nonlinear systems with parametric uncertainties," *IEEE Trans. Ind. Electron.*, vol. 55, no. 11, pp. 4029–4036, 2008.
[19] A. Levant, "Higher-order sliding modes, differentiation and output-feedback control," *International Journal of Control*, vol. 76, no. 9-10, pp. 924–941, 2003.
[20] J. Liu, S. Laghrouche, M. Harmouche, and M. Wack, "Adaptive-gain second-order sliding mode observer design for switching power converters," *Control Engineering Practice*, vol. 30, pp. 124–131, 2014.
[21] J. Liu, S. Laghrouche, and M. Wack, "Observer-based higher order sliding mode control of power factor in three-phase AC/DC converter for hybrid electric vehicle applications," *International Journal of Control*, vol. 87, no. 6, pp. 1117–1130, 2014.
[22] A. Ingimundarson, A. Stefanopoulou, and D. McKay, "Model-based detection of hydrogen leaks in a fuel cell stack," *IEEE Trans. Control Syst. Technol.*, vol. 16, no. 5, pp. 1004–1012, 2008.
[23] S. D. Lira, V. Puig, J. Quevedo, and A. Husar, "LPV observer design for PEM fuel cell system: application to fault detection," *J Power Sources*, vol. 196, no. 9, pp. 4298–4305, 2011.
[24] L. Zhang and A. Q. Huang, "Model-based fault detection of hybrid fuel cell and photovoltaic direct current power sources," *J Power Sources*, vol. 196, no. 11, pp. 5197–5204, 2011.
[25] S. Yin, H. Luo, and S. X. Ding, "Real-time implementation of fault-tolerant control systems with performance optimization," *IEEE Trans. Ind. Electron.*, vol. 61, no. 5, pp. 2402–2411, 2014.
[26] J.-H. Jung, S. Ahmed, and P. Enjeti, "PEM fuel cell stack model development for real-time simulation applications," *IEEE Trans. Ind. Electron.*, vol. 58, no. 9, pp. 4217–4231, 2011.
[27] J. A. Moreno and M. Osorio, "A Lyapunov approach to second-order sliding mode controllers and observers," in *47th IEEE Conference on Decision and Control(CDC)*. IEEE, 2008, pp. 2856–2861.
[28] W. Respondek, A. Pogromsky, and H. Nijmeijer, "Time scaling for observer design with linearizable error dynamics," *Automatica*, vol. 40, no. 2, pp. 277–285, 2004.
[29] K.-W. Suh and A. G. Stefanopoulou, "Performance limitations of air flow control in power-autonomous fuel cell systems," *IEEE Trans. Control Syst. Technol.*, vol. 15, no. 3, pp. 465–473, 2007.
[30] R. Talj, D. Hissel, R. Ortega, M. Becherif, and M. Hilairet, "Experimental validation of a PEM fuel-cell reduced-order model and a moto-compressor higher order sliding-mode control," *IEEE Trans. Ind. Electron.*, vol. 57, no. 6, pp. 1906–1913, 2010.
[31] A. Vahidi, A. Stefanopoulou, and H. Peng, "Current management in a hybrid fuel cell power system: A model-predictive control approach," *IEEE Trans. Control Syst. Technol.*, vol. 14, no. 6, pp. 1047–1057, 2006.
[32] J. T. Pukrushpan, A. G. Stefanopoulou, and H. Peng, *Control of fuel cell power systems: principles, modeling, analysis and feedback design*. Springer Science & Business Media, 2004.
[33] J. Larminie, A. Dicks, and M. S. McDonald, *Fuel cell systems explained*. Wiley New York, 2003, vol. 2.
[34] S. M. Rakhtala, A. R. Noei, R. Ghaderi, and E. Usai, "Design of finite-time high-order sliding mode state observer: A practical insight to PEM fuel cell system," *J Process Control*, vol. 24, no. 1, pp. 203–224, 2014.
[35] J. B. Heywood, *Internal combustion engine fundamentals*. New York: Mcgraw-hill, 1988, vol. 930.
[36] Y. She, M. Baran, and X. She, "Multiobjective control of PEM fuel cell system with improved durability," *IEEE Trans. Sustain. Energy*, vol. 4, no. 1, pp. 127–135, 2013.
[37] C. Ramos-Paja, R. Giral, L. Martinez-Salamero, J. Romano, A. Romero, and G. Spagnuolo, "A PEM fuel-cell model featuring oxygen-excess-ratio estimation and power-electronics interaction," *IEEE Trans. Ind. Electron.*, vol. 57, no. 6, pp. 1914–1924, 2010.
[38] X. Zhang, M. Polycarpou, and T. Parisini, "Fault diagnosis of a class of nonlinear uncertain systems with lipschitz nonlinearities using adaptive estimation," *Automatica*, vol. 46, no. 2, pp. 290–299, 2010.
[39] H. K. Khalil and J. Grizzle, *Nonlinear systems*. New Jersey: Prentice Hall, 1996, vol. 3.
[40] R. Talj, R. Ortega, and M. Hilairet, "A controller tuning methodology for the air supply system of a PEM fuel-cell system with guaranteed stability properties," *International Journal of Control*, vol. 82, no. 9, pp. 1706–1719, 2009.
[41] J. C. Amphlett, R. Baumert, R. F. Mann, B. A. Peppley, P. R. Roberge, and T. J. Harris, "Performance modeling of the Ballard Mark IV solid polymer electrolyte fuel cell II. Empirical model development," *J Electrochem Soc*, vol. 142, no. 1, pp. 9–15, 1995.

Jianxing Liu received the B.S. degree in mechanical engineering in 2004, the M.E. degree in control science and engineering in 2010, both from Harbin Institute of Technology, Harbin, China and the PhD degree in automation from the Technical University of Belfort-Montbeliard (UTBM), France, in 2014. Since 2014, he is with Harbin Institute of Technology, China.

His current research interests include sliding mode control, nonlinear control of power electronics systems and power electronics converters applied to renewable energy systems.

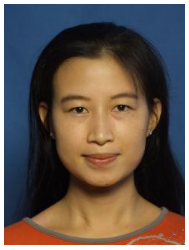

Wensheng Luo received the B.S. degree in Mechanical Design, Manufacturing and Automation from Harbin Engineering University, China, in 2007, the M.E. degree in Mechatronics from Harbin Institute of Technology, China, in 2009.

Wensheng Luo is currently a PhD student majoring in Control Theory and Control Engineering in Harbin Institute of Technology, China. Her current research interests include linear parameter-varying (LPV) systems, stochastic systems, model reduction, and observer design for power converters.

Xiaozhan Yang received the B.E. degree in electrical engineering and automation from Shijiazhuang Tiedao University, Shijiazhuang, China, in 2011; the M.E. degree in control science and engineering from Harbin Institute of Technology, China, in 2013. He is currently a PhD student in King's College London, London, United Kingdom. His current research interests include T-S fuzzy systems, robotics, and model reduction.

Ligang Wu (M'10-SM'12) received the B.S. degree in Automation from Harbin University of Science and Technology, China in 2001; the M.E. degree in Navigation Guidance and Control from Harbin Institute of Technology, China in 2003; the PhD degree in Control Theory and Control Engineering from Harbin Institute of Technology, China in 2006. From January 2006 to April 2007, he was a Research Associate in the Department of Mechanical Engineering, The University of Hong Kong, Hong Kong. From September 2007 to June 2008, he was a Senior Research Associate in the Department of Mathematics, City University of Hong Kong, Hong Kong. From December 2012 to December 2013, he was a Research Associate in the Department of Electrical and Electronic Engineering, Imperial College London, London, UK. In 2008, he joined the Harbin Institute of Technology, China, as an Associate Professor, and was then promoted to a Professor in 2012.

Dr. Wu currently serves as an Associate Editor for a number of journals, including IEEE TRANSACTIONS ON AUTOMATIC CONTROL, IEEE/ASME TRANSACTIONS ON MECHATRONICS, *Information Sciences*, *Signal Processing*, and *IET Control Theory and Applications*. He is also an Associate Editor for the Conference Editorial Board, IEEE Control Systems Society. Dr. Wu has published more than 100 research papers in international referred journals.

His current research interests include switched hybrid systems, computational and intelligent systems, sliding mode control, optimal filtering, and flight control.